Spacing-Dependent Antimicrobial Efficacy of Immobilized Silver Nanoparticles

ARTICLE *in* JOURNAL OF PHYSICAL CHEMISTRY LETTERS · FEBRUARY 2014

Impact Factor: 7.46 · DOI: 10.1021/jz5000269

4 AUTHORS, INCLUDING:

Huiliang Cao
Chinese Academy of Sciences
29 PUBLICATIONS **289** CITATIONS

SEE PROFILE

THE JOURNAL OF PHYSICAL CHEMISTRY Letters

Letter

pubs.acs.org/JPCL

Spacing-Dependent Antimicrobial Efficacy of Immobilized Silver Nanoparticles

Huiliang Cao,* Yuqin Qiao, Fanhao Meng, and Xuanyong Liu*

State Key Laboratory of High Performance Ceramics and Superfine Microstructure, Shanghai Institute of Ceramics, Chinese Academy of Sciences, Shanghai 200050, China

Supporting Information

ABSTRACT: Silver nanoparticles (Ag NPs) with a similar mean particle diameter (~5.0 nm) but distinguished dispersion densities were in situ fabricated and immobilized on plasma-sprayed titanium oxide coatings by a silver plasma immersion ion implantation process (Ag PIII). Experiments and theoretical predictions demonstrated that the efficacy of these Ag NPs against bacteria relies on their electron storage capability, which is the interparticle distance associated in the dark, and it is inversely dose-dependent. A particle population with a relatively large spacing distance is superior in concentrating the electrons extruded by bacterial cells, activating oxidative reactions, and disrupting the bacterial cells. The finding opens up a new window leading to active design and control of the interactions between materials and biological systems.

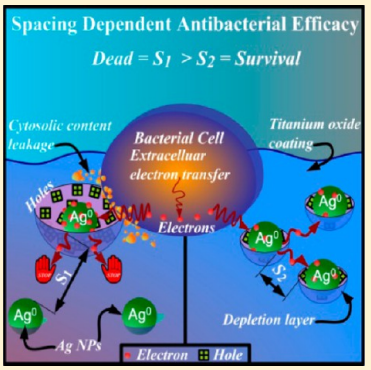

SECTION: Surfaces, Interfaces, Porous Materials, and Catalysis

Due to the ever-increasing incidence of persistent bacteria, there is a rising need to enhance our antimicrobial arsenal.[1] Silver nanoparticles (Ag NPs) are promising bullets in fighting against a broad spectrum of pathogenic microbes, including antibiotic-resistant strains,[2,3] yet the ultrasmall size and high mobility of Ag NPs also raise concerns about their potential toxicity to human health.[4,5] Especially, mobile Ag NPs may enter mammalian cells and damage the intracellular functions.[6,7] Accordingly, an important strategy to improve the compatibility of Ag NPs is to restrict the mobility of Ag NPs by immobilizing them on (or in) macrosurfaces,[8] prompting the research on revealing the antibacterial mechanisms of immobilized Ag NPs.

Since the report on the photolysis of water in the early 1970s,[9] titanium oxides have been extensively studied as catalysts for photolysis of bacteria and disinfection. It is generally recognized that the bactericidal action of titanium oxide is closely related to its light-induced charge separation processes, which produce "hole pools" (h^+) that can react directly with the bacterial membrane in contact or indirectly by reacting with adsorbed hydroxide ions (OH^-) and producing oxidative species (such as hydroxyl radicals, $OH^\bullet$, and hydrogen peroxide, H_2O_2), leading to chemical transformation of the biomolecules.[10,11] Thus, a minimum photonic energy that likely equals the band gap energy of the material is required in exciting the charge separation processes. This is why ultraviolet (UV) light is usually required in activating the antibacterial capacity of titanium dioxide. In order to decrease the threshold, band gap narrowing procedures are normally applied on the material. Among these strategies, loading of noble metals, such as silver (Ag), will endow the material with a rectifying electron-transfer property and facilitate the electron/hole separation processes in titanium oxide.[12,13] Despite abundant of studies on utilizing the charge separation behavior of Ag-loaded titanium oxide for visible-light-responsive disinfection,[14] its nonradiative property is seldom concerned. In fact, the direct consequence in the absence of light is that the irradiation-induced charge separation processes were ruled out, and the subsequent hole-pool-stimulated reactions do not occur.[15,16] However, extracellular electron transfer is a general mechanism in which the bacteria generate energy for cell growth and/or maintenance.[17−19] Accordingly, Ag NPs may collect bacteria-extruded electrons by taking advantage of the rectifying electron-transfer behavior of Ag NP/titanium oxide contacts and induce valence band hole (h^+) accumulation at the titanium oxide side adjacent to the interfaces, damaging to bacterial cells similar to that under light illumination.

Accordingly, in this study, immobilized Ag NPs with similar size distributions but different dispersion densities were fabricated on the surfaces of titanium oxide coating (TOC) by a Ag plasma immersion ion implantation process (Ag PIII). We found that the antibacterial efficacy of these Ag NPs depends on the interparticle distance, which is inversely correlated with the dose increases of Ag. A particle population with a relatively large spacing distance facilitates disrupting the integrity of the bacterial membrane. The results demonstrated

Received: January 6, 2014
Accepted: February 4, 2014

   dx.doi.org/10.1021/jz5000269 | J. Phys. Chem. Lett. 2014, 5, 743−748

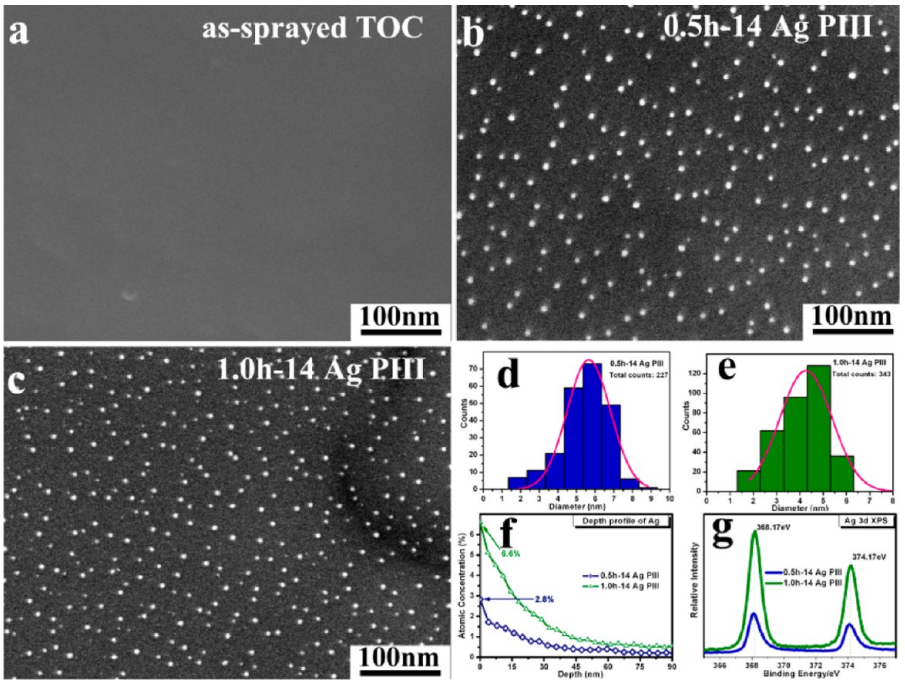

Figure 1. SEM images of the as-sprayed TOC (a), 0.5h-14 Ag PIII (b), and 1.0h-14 Ag PIII (c); particle size (diameter) distribution profiles of the 0.5h-14 Ag PIII (d) and 1.0h-14 Ag PIII (e); XPS depth profiles of Ag (f) and the Ag 3d XPS spectra (g) for the two Ag PIII samples.

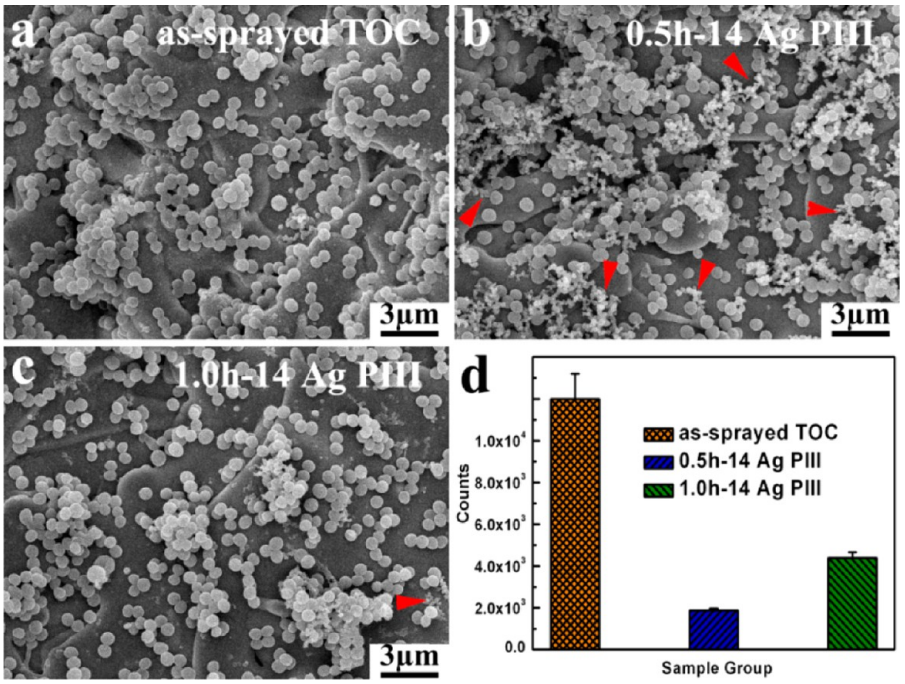

Figure 2. SEM morphologies of the *S. aureus* cells cultivated in the dark for 24 h on as-sprayed TOC (a), 0.5h-14Ag PIII (b), 1.0h-14Ag PIII (c), and counts of the recultivated bacterial colonies on agar (d); *S. aureus* colonies were previously dissociated from as-sprayed TOC, 0.5h-14Ag PIII, and 1.0h-14Ag PIII.

that we can fabricate antibacterial coatings with enhanced efficacy but fewer Ag NPs.

The fabrication procedure of immobilized Ag NPs is schematically shown in Scheme S1 (Supporting Information). First, a titanium oxide layer was plasma-sprayed onto titanium substrates. Then, the titanium oxide layer was treated by a Ag PIII at room temperature. During the Ag PIII, immobilized Ag NPs with a similar size distribution but different spacing distances (denoted by the surface to surface distance between particles, *S*) precipitate in the titanium oxide layer. Figure 1a–c shows typical scanning electron microscopy (SEM) images of the titanium oxide layer before and after Ag PIII. It can be seen that the as-sprayed TOC, rough in microscale (Figure S1, Supporting Information) but smooth in nanoscale (Figure 1a), comprises a mixture of anatase, rutile, and reduced phases of titanium oxide according to the powder X-ray diffraction

dx.doi.org/10.1021/jz5000269 | *J. Phys. Chem. Lett.* 2014, 5, 743–748

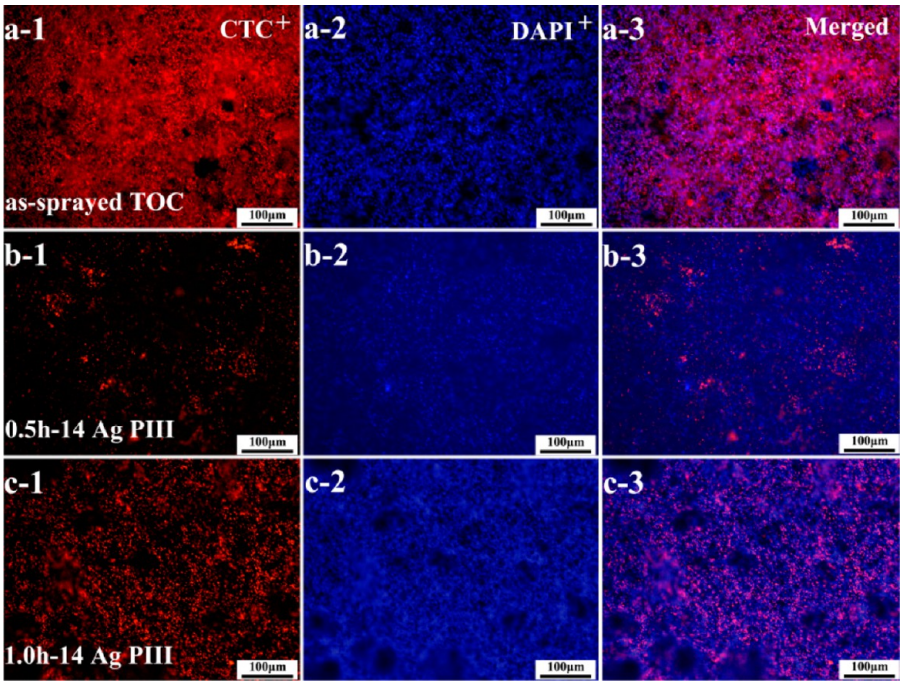

Figure 3. Fluorescence microscopy images of CTC-reducing bacteria together with Dapi-counter stained cells in the same area. (i-1) is CTC-positive, (i-2) is Dapi-positive in the same area, and (i-3) is the merged images of CTC and Dapi-positive. i = a, b, and c represent as-sprayed TOC, 0.5h-14 Ag PIII, and 1.0h-14 Ag PIII, respectively.

spectrum (Figure S2, Supporting Information). NPs can be detected on the TOC after being Ag PIII treated at 14 kV for 0.5 h (Figure 1b, denoted as 0.5h-14 Ag PIII) and 1.0 h (Figure 1c, denoted as 1.0h-14 Ag PIII). The particles on both Ag PIII samples are nearly monodispersed with a similar mean particle size (diameter) of about 5.0 nm (Figures 1d,e), but their dispersion densities are different between each other. It is about 0.97×10^3 (particles per square micrometer) for 0.5h-14 Ag PIII, while it is about 1.47×10^3 for1.0h-14 Ag PIII. This is qualitatively consistent with the evolution of Ag concentration obtained by X-ray photoelectron spectroscopy (XPS), as shown in Figure 1f; the Ag concentration in the outer surface of 0.5h-14 Ag PIII is 2.8 atom %, while that of 1.0h-14 Ag PIII is 6.60 atom %. However, the XPS Ag 3d spectra showed no noticeable binding energy shift between the two Ag PIII samples (Figure 1g). The Ag 3d doublet at 374.2 eV (Ag 3d3/2) and 368.2 eV (Ag 3d5/2) corresponds to metallic Ag.[20]

To evaluate the antimicrobial efficiency of the Ag PIII samples, *Staphylococcus aureus* (*S. aureus*) cells are introduced onto the as-sprayed (control) and Ag PIII (the 0.5h-14 Ag PIII and 1.0h-14 Ag PIII) samples and incubated at 37 °C for 24 h in the dark (in order to eliminate the photocatalytic biocide effects of titanium oxide). As shown in Figure 2, the bacterial cells on the as-sprayed sample were normal without apparent damage (Figure 2a), but cytosolic content leakage on 0.5h-14 Ag PIII prevailed (see the arrow in Figure 2b; the higher magnification image is shown in Figure S3, Supporting Information), and it happens occasionally on 1.0h-14 Ag PIII (arrowed in Figure 2c), indicating that the antibacterial activity of these Ag NPs lies in disrupting the integrity of the bacterial membrane. In order to quantitatively evaluate the bactericidal efficacy of the Ag PIII samples, the attached bacteria were detached and recultivated on agar according to the bacteria counting method. The reduction rate for 1.0h-14 Ag PIII is below 70%, whereas that for 0.5h-14 Ag PIII reaches 90% (Figure 2d), which is consistent with the SEM observations in Figure 2b and c, demonstrating that the antimicrobial efficacy for 0.5h-14 Ag PIII is superior to that for 1.0h-14 Ag PIII.

The result was further confirmed by evaluating the bacterial viability using the 5-cyano-2,3-ditolyl tetrazolium chloride (CTC) assay. CTC is a kind of tetrazolium dye that is thought to act as an alternative electron acceptor and, consequently, can be reduced by respiring bacterial cells to water-insoluble formazan product 3-cyan-1,5-ditolyl-formazan (CTF), a red fluorescent. As shown in Figure 3, the numbers of CTC-positive bacteria on 1.0h-14 Ag PIII (Figure 3(c-1)) was typically larger than that on 0.5h-14 Ag PIII (Figure 3(b-1)), indicating that the damage of the respiratory electron-transport system for the bacterial cells on 0.5h-14 Ag PIII is more serious than that on 1.0h-14 Ag PIII, which is consistent with the results presented in Figure 2, showing that cytosolic content leakage on the 0.5h-14 Ag PIII is more prevalent than that on 1.0h-14 Ag PIII.

It is believed that the antibacterial efficacy of these immobilized Ag NPs relies on their electron-transfer behavior. The electron storage capability of the Ag PIII samples in air was evidenced by their decreased photoluminescence signals as compared with that of as-sprayed TOC (Figure S4, Supporting Information). However, this evidence alone is not adequate in exactly uncovering the nature of electron storage on Ag PIII samples, which are immersed in a solution as culturing of bacteria in the dark (without light illumination). In fact, extracellular electron transfer is a general process in bacteria,[17−19] and it likely serves as an electron source in the dark. Nevertheless, the extracellular electron-transfer process of bacteria is not easy to be checked because of the small size of those membrane organelles involved (Figure S5, Supporting Information). Even so, it is noted that chromosomal deoxyribonucleic acid (DNA) is specifically attached to the bacterial cell membrane to maintain its proper localization, and

dx.doi.org/10.1021/jz5000269 | *J. Phys. Chem. Lett.* 2014, 5, 743−748

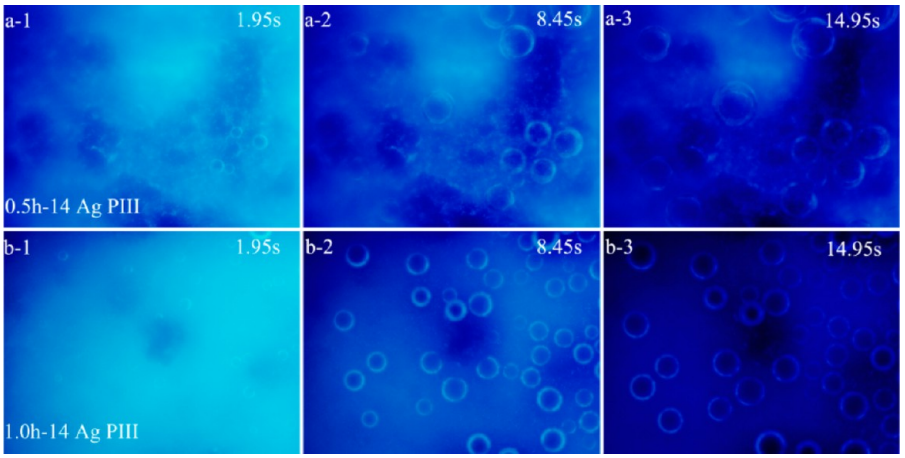

Figure 4. A series of frames captured with a fluorescence microscope depicting the kinetics of fluorescence dye quenching and gas bubble bursting from the Ag PIII samples illuminated with UV for about 1.95 s (j-1), 8.45 s (j-2), and 14.95 s (j-3); j = a and b represent 0.5h-14 Ag PIII and 1.0h-14 Ag PIII, respectively. For details, please watch the corresponding Movies S1 (jz5000269_si_002.avi) and S2 (jz5000269_si_003.avi) in the Supporting Information.

this structure may be used to mimic the electron extrusion process of bacterial cells. Accordingly, a fluorescence procedure was developed to track the electron-transfer process of immobilized Ag NPs. That is, the bacterial chromosome was stained by a DNA minor groove binder, Hoechst 33342 (a blue dye with excitation/emission light of ~350/461 nm).[21] By UV-exciting the dye, extra electrons can be produced and injected across the bacterial membrane onto the surfaces of the Ag PIII samples, which were immersed in a glycerol solution containing 10% water (Figure S6, Supporting Information). As the results shown in Figure 4 (Movies S1 (jz5000269_si_002.avi) and S2 (jz5000269_si_003.avi), Supporting Information), fluorescence dye (blue light) quenching and air bubble formation can be observed on the two Ag PIII samples, but both the fluorescence dye quenching and air bubble formation on 1.0h-14 Ag PIII are faster than that on 0.5h-14 Ag PIII. The results suggest that the electron storage capability of 1.0h-14 Ag PIII in a solution is inferior to that of 0.5h-14 Ag PIII, though both samples receive electrons from bacterial cells.

The aforementioned results demonstrate that more Ag NPs does not guarantee good antibacterial efficacy, which is unexpectedly inconsistent with the results in the literature, indicating that the antibacterial activity of Ag NPs is positively dose-dependent (more Ag means better efficacy).[22−24] However, the finding can be explained from the electrostatic interaction viewpoint. As the Ag PIII procedure is prolonged, the population of Ag NPs (typically arranged in a nearest or in a line manner, Figures S7 and S8, Supporting Information) in the TOC increases, and the average spacing distance decreases. As a result, the interparticle capacitances should be taken into account because a charged Ag NP particle may polarize its neighbors.[25] For those arranged in a nearest manner, one Ag NP typically has three nearest neighbors (this is true according to Figure S7, Supporting Information), and the interparticle capacitance C can be estimated to be about 6.2 aF using[26,27]

$$C \approx \pi\varepsilon_0\varepsilon D \ln\left(1 + \frac{D}{S}\right) \quad (1)$$

where D is the particle diameter (~5 nm), S is the interparticle distance (set to be 10 nm), ε_0 is the permittivity of vacuum, and ε is the dielectric constant of titanium dioxide (~100[28]). Therefore, the activation energy $E_C \approx 4.4$ meV for charging of the three nearest neutral Ag NPs can be determined by[26,27]

$$E_C = \frac{e^2}{2C_\Sigma} \quad (2)$$

Here, e is the elementary electronic charge of the electron, and C_Σ is the sum of the three interparticle capacitances (~18.6 aF). An energy (~4.4 meV) of only about 1/30 of that of a bacterial cell can be supplied (the membrane potential, $\Delta\phi$, in *S. aureus* is about −130 mV[29]). Moreover, the energy supplied by a bacterial cell could charge a maximum of 10 Ag NPs that are arranged in a line with an interparticle distance of 10 nm (in this case, C_Σ can be calculated as ~0.62 aF according to eq 2, which is about 1/10 of the interparticle capacitance estimated by eq 1, ~6.2 aF). The number is larger than the highest record (~6) that can be detected in the present study (arrowed in Figure S7b, Supporting Information). These results indicate that an adhered bacterium may not only charge the first nearest Ag NPs but also charge the second nearest neighbors (even the third or the fourth) through the first ones as the particles get close enough, implying the possibility of electron leakages on the first nearest Ag NPs while there are second nearest neighbors nearby. Counts for interparticle distances less than 10 nm on 1.0h-14 Ag PIII are over six times larger than those on 0.5h-14 Ag PIII, indicating that the chance for electron leakage on 1.0h-14 Ag PIII is higher than that on 0.5h-14 Ag PIII. This was evidenced by directly UV-illuminating the Hoechst 33342-stained samples (do not immerse the sample in the glycerol solution). The results demonstrate that fluctuations of fluorescence dye quenching (the fluorescence intensity occasionally increases as the UV illumination proceeds) can easily be detected on 0.5h-14 Ag PIII (Figure S9 and Movie S3 (jz5000269_si_004.avi), Supporting Information) but hardly on 1.0h-14 Ag PIII (Movie S4 (jz5000269_si_005.avi), Supporting Information). In short, Ag NPs on 0.5h-14 Ag PIII tend to concentrate the received electrons and stimulate oxidative stress strong enough in disrupting membrane integrity of bacterial cells and inducing cytosolic content leakage (Figure 2). This is in good agreement with the results in the literature, which indicated that to increase the probability of pore

dx.doi.org/10.1021/jz5000269 | J. Phys. Chem. Lett. 2014, 5, 743−748

formation in a bacterial membrane, one should increase the peroxidation strength.[30]

In summary, Ag NPs with a similar mean diameter (~5.0 nm) but distinguished dispersion densities were in situ fabricated and immobilized on plasma-sprayed TOCs by a Ag PIII process. Experiments and theoretical predictions indicate that the efficacy of these Ag NPs against bacteria relies on their electron storage nature, which is associated with the interparticle distance in the dark. The finding opens up a new window leading to active design and control of the interactions between materials and biological systems, and it is significant in boosting the efficiency of nanostructural materials for biomaterials, catalysts, and sensors.

■ ASSOCIATED CONTENT

Supporting Information

Experimental details and additional data, including a schematic illustration for fabricating immobilized Ag NPs on a titanium oxide coating, low-magnification SEM morphology of the as-sprayed titanium oxide coating, X-ray diffraction spectrum of the as-sprayed titanium oxide coating, higher magnification SEM morphologies of the *S. aureus* cells cultivated in the dark, photoluminescence spectra of the as-sprayed and Ag PIII treated titanium oxide coating, schematic illustration for how an adhered bacteria induces oxidation reactions on Ag PIII samples in the dark, schematic illustration for how to mimic the electron extrusion process of bacterial cells, counts of the interparticle distances less than 10 nm for the immobilized Ag NPs, schematic illustration of the electron-transfer paths for the two typical arrangements concerned, a series of frames depicting the fluctuations of fluorescence dye quenching, details of the Ag PIII parameters for the samples involved, movies of the fluctuations of fluorescence dye quenching and air bubble formation, and experimental details for plasma spraying of titanium oxide coating, silver plasma immersion ion implantation, sample surface chemistry and structure characterization, antibacterial efficacy evaluation, chromosomal DNA staining, tracking the electron storage capability of immobilized Ag NPs, and Antibacterial Action of Immobilized Ag NPs. This material is available free of charge via the Internet at http://pubs.acs.org.

■ AUTHOR INFORMATION

Corresponding Authors

*E-mail: hlc@mail.sic.ac.cn (H.C.).
*E-mail: xyliu@mail.sic.ac.cn (X.L.).

Notes

The authors declare no competing financial interest.

■ ACKNOWLEDGMENTS

This work was jointly supported by the National Basic Research Program of China (973 Program, 2012CB933600), the National Natural Science Foundation of China (31100675 and 31370962), the Shanghai Science and Technology R&D Fund (11JC1413700), the Science Foundation for Youth Scholar of State Key Laboratory of High Performance Ceramics and Superfine Microstructures (SKL201103), and the Innovation Fund of SICCAS (Y26ZC3130G).

■ REFERENCES

(1) Taubes, G. The Bacteria Fight Back. *Science* **2008**, *321*, 356−361.
(2) Eckhardt, S.; Brunetto, P. S.; Gagnon, J.; Priebe, M.; Giese, B.; Fromm, K. M. Nanobio Silver: Its Interactions with Peptides and Bacteria, and Its Uses in Medicine. *Chem. Rev.* **2013**, *113*, 4708−4754.
(3) Chernousova, S.; Epple, M. Silver as Antibacterial Agent: Ion, Nanoparticle, and Metal. *Angew. Chem., Int. Ed.* **2013**, *52*, 1636−1653.
(4) Nowack, B. Nanosilver Revisited Downstream. *Science* **2010**, *330*, 1054−1055.
(5) Hansen, S. F.; Baun, A. When Enough is Enough. *Nat. Nanotechnol.* **2012**, *7*, 409−411.
(6) AshaRani, P. V.; Mun, G. L. K.; Hande, M. P.; Valiyaveettil, S. Cytotoxicity and Genotoxicity of Silver Nanoparticles in Human Cells. *ACS Nano* **2009**, *3*, 279−290.
(7) Pratsinis, A.; Hervella, P.; Leroux, J. C.; Pratsinis, S. E.; Sotiriou, G. A. Toxicity of Silver Nanoparticles in Macrophages. *Small* **2013**, *9*, 2576−2584.
(8) Campoccia, D.; Montanaro, L.; Arciola, C. R. A Review of the Biomaterials Technologies for Infection-Resistant Surfaces. *Biomaterials* **2013**, *34*, 8533−8554.
(9) Fujishima, A.; Honda, K. Electrochemical Photolysis of Water at a Semiconductor Electrode. *Nature* **1972**, *238*, 37−38.
(10) Sunada, K.; Kikuchi, Y.; Hashimoto, K.; Fujishima, A. Bactericidal and Detoxification Effects of TiO_2 Thin Film Photocatalysts. *Environ. Sci. Technol.* **1998**, *32*, 726−728.
(11) Valentin, C. D.; Fittipaldi, D. Hole Scavenging by Organic Adsorbates on the TiO_2 Surface: A DFT Model Study. *J. Phys. Chem. Lett.* **2013**, *4*, 1901−1906.
(12) Zhang, Z.; Yates, J. T. Band Bending in Semiconductors: Chemical and Physical Consequences at Surfaces and Interfaces. *Chem. Rev.* **2012**, *112*, 5520−5551.
(13) Takai, A.; Kamat, P. V. Capture, Store, and Discharge. Shuttling Photogenerated Electrons Across TiO_2−Silver Interface. *ACS Nano* **2011**, *5*, 7369−7376.
(14) Henderson, M. A. A Surface Science Perspective on TiO_2 Photocatalysis. *Surf. Sci. Rep.* **2011**, *66*, 185−297.
(15) Akimov, A. V.; Neukirch, A. J.; Prezhdo, O. V. Theoretical Insights into Photoinduced Charge Transfer and Catalysis at Oxide Interfaces. *Chem. Rev.* **2013**, *113*, 4496−4565.
(16) Bian, Z.; Tachikawa, T.; Majima, T. Superstructure of TiO_2 Crystalline Nanoparticles Yields Effective Conduction Pathways for Photogenerated Charges. *J. Phys. Chem. Lett.* **2012**, *3*, 1422−1427.
(17) Reguera, G.; McCarthy, K. D.; Mehta, T.; Nicoll, J. S.; Tuominen, M. T.; Lovley, D. R. Extracellular Electron Transfer via Microbial Nanowires. *Nature* **2005**, *435*, 1098−1101.
(18) Harris, H. W.; El-Naggar, M. Y.; Bretschger, O.; Ward, M. J.; Romine, M. F.; Obraztsova, A. Y.; Nealson, K. H. Electrokinesis is a Microbial Behavior that Requires Extracellular Electron Transport. *Proc. Natl. Acad. Sci. U.S.A.* **2010**, *107*, 326−331.
(19) Okamoto, A.; Hashimoto, K.; Nealson, K. H.; Nakamura, R. Rate Enhancement of Bacterial Extracellular Electron Transport Involves Bound Flavin Semiquinones. *Proc. Natl. Acad. Sci. U.S.A.* **2013**, *110*, 7856−7861.
(20) Chastain, J. *Handbook of X-ray Photoelectron Spectroscopy*; Perkin-Elmer Corporation: Eden Prairie, MN, 1992.
(21) Zhang, X.; Zhang, S. C.; Sun, D.; Hu, J.; Wali, A.; Pass, H.; Fernandez-Madrid, F.; Harbut, M. R.; Tang, N. New Insight into the Molecular Mechanisms of the Biological Effects of DNA Minor Groove Binders. *PLoS One* **2011**, *6*, e25822.
(22) Ragaseema, V. M.; Unnikrishnan, S.; K.Krishnan, V.; Krishnan, L. K. The Antithrombotic and Antimicrobial Properties of PEG-Protected Silver Nanoparticle Coated Surfaces. *Biomaterials* **2012**, *33*, 3083−3092.
(23) Alarcon, E. I.; Udekwu, K.; Skog, M.; Pacioni, N. L.; Stamplecoskie, K. G.; González-Béjar, M.; Polisetti, N.; Wickham, A.; Richter-Dahlfors, A.; Griffith, M.; et al. The Biocompatibility and Antibacterial Properties of Collagen-Stabilized, Photochemically Prepared Silver Nanoparticles. *Biomaterials* **2012**, *33*, 4947−4956.
(24) Guo, D.; Zhu, L.; Huang, Z.; Zhou, H.; Ge, Y.; Ma, W.; Wu, J.; Zhang, X.; Zhou, X.; Zhang, Y.; et al. Anti-leukemia Activity of PVP-

Coated Silver Nanoparticles via Generation of Reactive Oxygen Species and Release of Silver Ions. *Biomaterials* **2013**, *34*, 7884−7894.
(25) Zabet-Khosousi, A.; Dhirani, A. A. Charge Transport in Nanoparticle Assemblies. *Chem. Rev.* **2008**, *108*, 4072−4124.
(26) Black, C. T.; Murray, C. B.; Sandstrom, R. L.; Sun, S. Spin-Dependent Tunneling in Self-Assembled Cobalt-Nanocrystal Superlattices. *Science* **2000**, *290*, 1131−1134.
(27) Beecher, P.; Quinn, A. J.; Shevchenko, E. V.; Weller, H.; Redmond, G. Insulator-to-Metal Transition in Nanocrystal Assemblies Driven by In Situ Mild Thermal Annealing. *Nano Lett.* **2004**, *4*, 1289−1293.
(28) Diebold, U. The Surface Science of Titanium Dioxide. *Surf. Sci. Rep.* **2003**, *48*, 53−229.
(29) Mates, S. M.; Eisenberg, E. S.; Mandel, L. J.; Patel, L.; Kaback, H. R.; Miller, M. H. Membrane Potential and Gentamicin Uptake in Staphylococcus Aureus. *Proc. Natl. Acad. Sci. U.S.A.* **1982**, *79*, 6693−6697.
(30) Gurtovenko, A. A.; Anwar, J.; Vattulainen, I. Defect-Mediated Trafficking Across Cell Membranes: Insights from In Silico Modeling. *Chem. Rev.* **2010**, *110*, 6077−6103.